J. Fluid Mech. (2011), *vol.* 689, *pp.* 254–278.
doi:10.1017/jfm.2011.413

Turbulent fountains in one- and two-layer crossflows

Joseph K. Ansong[1], Alexandra Anderson-Frey[2] and Bruce R. Sutherland[1,2]†

[1] Department of Physics, University of Alberta, Edmonton, AB, T6G 2E1, Canada

[2] Department of Earth and Atmospheric Sciences, University of Alberta, Edmonton, AB, T6G 2E3, Canada

(Received 21 June 2011; revised 14 September 2011; accepted 20 September 2011; first published online 8 November 2011)

The Lagrangian theory developed for fountains in a stationary fluid is extended to predict the path and breadth of a fountain in a one- and two-layer fluid with a moderate crossflow. The predictions compare well with the results of laboratory experiments of fountains in a one-layer fluid. The empirical spreading parameter determined from the one-layer experiments is used in the theory for fountains in a two-layer crossflow. Though qualitatively correct, the theory underpredicts the height and radius of the fountains. Similar to the behaviour of fountains in two-layer stationary ambients, the fountain in a two-layer crossflow is observed to exhibit three regimes of flow: it may penetrate the interface, eventually returning to the level of the source where it spreads as a propagating gravity current; upon descent, it may be trapped at the interface where it spreads as a propagating intrusion; it may do both, partially descending to the source and partially being trapped at the interface. These regimes are classified theoretically and empirically. The theoretical classification compared the buoyancy excess of the descending flow to the density difference between the two layers. The regimes are also classified using empirically determined regime parameters which govern the relative initial momentum of the fountain and the relative density difference of the fountain and the ambient fluid.

Key words: plumes/thermals

1. Introduction

Negatively buoyant plumes, or fountains, are formed either when dense fluid is continuously discharged upward into a less dense fluid or when less dense fluid is continuously discharged downward into a more dense environment (Morton 1959). In either case, buoyancy opposes the momentum of the flow until the fountain reaches a height where the vertical velocity goes to zero. The fountain then reverses direction and, in the absence of any background horizontal flow, returns toward the source. In the presence of a crossflow, the fountain returns some horizontal distance away from the source. Depending upon the strength of the crossflow, the returning fluid may or may not interact significantly with the fluid emanating from the source.

The release of fluid heavier than the environment with or without a crossflow has wide applications in the atmosphere, oceans and industry. The dispersion in the

† Email address for correspondence: bruce.sutherland@ualberta.ca

atmosphere of noxious gases heavier than air has important consequences on health (Britter & Griffiths 1982). Particularly disastrous cases include the release of dioxin in Seveso, Italy in 1976 and the leak calamity in Bhopal, India in 1984 (Britter 1989). A review of the circumstances surrounding some accidents as a result of the release of heavier-than-air gases has also been recorded by McQuaid (1989). Fountains also result from the discharge of effluents into water bodies. In particular, sea water desalination usually results in the upward discharge of concentrated salt solutions below the sea surface (Roberts & Toms 1987).

In the case of upwardly directed fountains, the initially rising segment of the fountain is often more stable (with density decreasing upward) while the later descending return-flow is unstable in the sense that heavier fluid overlies lighter fluid. This gravitational instability causes the upper extreme of the fountain to be well defined while the descending flow is not due to fluid 'leaking' out of the main flow (Lane-Serff, Linden & Hillel 1993; Lindberg 1994; Gungor & Roberts 2009). These types of flows are sometimes referred to as dense jets, dense gas plumes, dense plumes or heavy gas jets (Britter & Griffiths 1982; Fay & Zemba 1986; Shaver & Forney 1988; Schatzmann, Snyder & Lawson 1993; Gungor & Roberts 2009).

One of the first experimental studies of fountains in a crosswind was by Bodurtha (1961), who conducted small-scale experiments to understand the environmental impact of the release of heavier-than-air gases from tall stacks into the atmosphere. Using dimensional analysis, they derived simple formulae to predict the maximum height and downward acceleration of the descending plumes. Measurements of the dilution of the plume at the ground were not made but estimates were obtained by assuming that the plume had a circular cross-section when it hits the ground.

The applicability of their expression for the maximum rise height was questioned by Hoot, Meroney & Peterka (1973). They conducted wind-tunnel studies of fountains in a laminar crossflow and also derived semi-empirical relations following the theory of positively buoyant plumes to match their results. They provided expressions for the concentration at the point of maximum rise and at the point where the centreline touched the ground. They also observed that the cross-section of the fountain at the maximum height was semi-elliptical and, as the plume descended, the cross-section became more nearly circular and the vertical distribution of concentration became more symmetrical.

Chu (1975) extended the theory on buoyant forced plumes developed by Chu & Goldberg (1974) to the case of fountains in a laminar crossflow. The theory made use of a single entrainment parameter to close the system of equations and it also assumed that the horizontal velocity component of the plume was approximately equal to the crossflow speed. The latter assumption required the plume to be well bent-over for the equations to be applicable (Roberts & Toms 1987). The resulting formulae predicted the trajectory of the fountain, its maximum rise height and its dilution as a function of downwind distance.

One of the most extensive experimental studies on vertical and inclined fountains in a crossflow was by Roberts & Toms (1987). Most of their experiments considered the case of a fountain inclined at an angle of 60° to the horizontal in a current flowing at different angles to the nozzle. They analysed the results using dimensional analyses and length scale arguments and presented the results in terms of the Froude number $Fr_b = (\pi/4)^{1/4}\, U_a/U_0$, in which U_a is the crossflow speed and $U_0 = M_0^{-1/4} F_0^{1/2}$ is a measure of the average vertical speed of the fountain from source to maximum rise. Here F_0 and M_0 are the buoyancy and momentum fluxes, respectively, at the source. The maximum rise of vertical fountains was found to be strongly dependent

on Fr_b being nearly constant for $0.2 < Fr_b < 0.8$ and decreasing with $Fr_b \gtrsim 0.8$. For $Fr_b \lesssim 0.2$ the fountain falls back upon the source flow.

Using three-dimensional laser-induced fluorescence (LIF) measurements to examine the dynamics of a fountain in a crossflow, Gungor & Roberts (2009) additionally measured the horizontal distance of the impingement point from the source. Their study revealed that the nature of the flow is more complex than previously thought. In particular, with $Fr_b = 0.9$ the descending flow was found to develop two counter-rotating vortices like those in a line thermal. These caused the downflow to bifurcate upon impinging the ground. Their results were similar to those presented in Roberts & Toms (1987) in that the maximum rise heights were predicted by the same equations but with larger empirical constants determining the dilution of the flow.

Shaver & Forney (1988) theoretically modelled dense gas plumes by altering the positively buoyant plume model developed by Hoult, Fay & Forney (1969). The theory is an extension of the pioneering Eulerian theory of Morton, Taylor & Turner (1956) but closes the system of equations with two empirical entrainment parameters. The properties of the fountain are then obtained along the centreline by numerically integrating the system of equations. Shaver & Forney (1988) also obtained asymptotic solutions of the equations for the maximum rise height, the impingement point and the dilution at the impingement point as functions of the stack height and the downwind distance.

In all these studies, the ambient fluid had uniform density. The work presented here is the next stage of a research program motivated in part to understand the evolution of dense pollutants that disperse in the presence of an atmospheric inversion. The first stage reported upon the behaviour of fountains in a two-layer stagnant ambient (Ansong, Kyba & Sutherland 2008). As in that work, a similar approach is followed here but with the additional consideration of a crossflow.

Although the generic problem of a fountain impinging upon an interface in a two-layer fluid with crossflow has a broad range of applications, our study is motivated by the long-range goal of understanding the dispersion of pollutants from sour gas flares in the presence of an atmospheric inversion. Sour gas flares contain high concentrations of hydrogen sulphide (H_2S), whose molecular mass is greater than that of air and which is deadly in concentrations as low as hundreds of parts per million. Flaring attempts to combust the gas, converting it into relatively benign sulphuric acid and other compounds. But studies have shown that a crosswind can significantly reduce combustion efficiency (Johnson & Kostiuk 2000). At present it is unknown in what concentrations the unburned and cooled gas returns to the ground. Predictions made using the dispersion codes such as AERMOD and CALPUFF do not account for fountain dynamics and only heuristically include the influence of atmospheric inversions.

Here we do not consider the thermodynamics of the heating and cooling of the gas. Instead we focus on the fundamental problem of a fountain in a moving stratified ambient. When a fountain impinges upward upon a two-layer fluid, the descending flow may return to the level of the source, it may become trapped at the density interface or it may do both. In any case, the descending flow then goes on to spread horizontally outward as a propagating gravity current.

The dynamics of fountains in a two-layer crossflow are virtually absent in the literature. Shiau, Yang & Tsai (2007) conducted two experiments of fountains in a two-layer crossflow and concluded that the terminal rise height decreases when the crossflow speed increases. Here we explore a broader parameter space in the

examination of two-layer crossflows and we extend the theory for fountains in a stationary two-layer fluid to include the effect of moderate crossflow speeds.

In § 2 we develop a simple theory for fountains in a uniform crossflow and we then extend it to the case of fountains in a two-layer crossflow in § 3. In § 4 we describe the set-up of the laboratory experiments and present qualitative results. In § 5 quantitative results from the experiments are presented. We analyse the classification of the flow regimes theoretically and empirically and we compare the measured quantities to the theoretical predictions. In § 6 we summarize the results.

2. Theory for fountains in a uniform ambient

Here we extend the Lagrangian theory for fountains in stationary environments (Lee & Chu 2003; Ansong *et al.* 2008) to include the effects of a moderate uniform crossflow. Although the Lagrangian and Eulerian integral method both give the same result (but with different empirical parameters) when applied to plumes, the Lagrangian method is simpler to compute and interpret applied to fountains (Lee & Chu 2003). First we review the theory for fountains in a stationary environment and then we extend it to include a uniform crossflow. Throughout, the theory is developed for a Boussinesq fluid in which the source fluid is injected upward into an ambient fluid of moderately smaller density.

2.1. *Fountains in stationary environments*

The Lagrangian approach tracks a rising slab of fluid that expands as a result of entrainment of ambient fluid. Assuming a top-hat-shaped fountain of radius r and mean vertical velocity w, we can write the volume, vertical momentum and buoyancy fluxes, respectively, as

$$Q = \pi r^2 w, \quad M = \pi r^2 w^2 \quad \text{and} \quad F = F_0 = \pi r^2 w g' = \pi r_0^2 w_0 {g_0}', \tag{2.1}$$

in which $g' = (\varrho - \rho_a)g/\rho_0$ is the reduced gravity within the fountain, ${g_0}' = g(\rho_0 - \rho_a)/\rho_0$ is the reduced gravity at the source, r_0 is the source radius, w_0 is the average vertical velocity at the source, ρ_a is the ambient density, $\varrho \equiv \varrho(t)$ is the density of a slab within the fountain at time t and $\rho_0 = \varrho(0)$ is the density of the fluid emanating from the source.

In a uniform ambient the buoyancy flux $F = F_0$ is constant. Conservation of momentum implies that the momentum flux of the slab changes in time due to the buoyancy flux:

$$\frac{\mathrm{d}M}{\mathrm{d}t} = -F_0. \tag{2.2}$$

The Lagrangian approach further makes the 'spreading hypothesis' that the fountain spreads linearly with height:

$$\frac{\mathrm{d}r}{\mathrm{d}z} = \beta, \tag{2.3}$$

in which z is the vertical coordinate and β is an empirically determined spreading coefficient. In the case of a fountain in a still ambient, Lee & Chu (2003) found $\beta \approx 0.17$.

Because F_0 is constant, equation (2.2) dictates that the momentum flux of a slab changes linearly in time according to

$$M = M_0 - F_0 t. \tag{2.4}$$

Rewriting (2.3) as $\mathrm{d}r/\mathrm{d}t = \beta w$, using (2.1) to write w in terms of M and using (2.4) gives a differential equation for $r(t)$. Solving with the initial condition $r(0) = r_0$ gives

$$r(t) = \left\{ r_0^2 + \left(\frac{4\beta}{3\sqrt{\pi}}\right) \frac{M_0^{3/2}}{F_0} \left[1 - \left(1 - \frac{F_0 t}{M_0} \right)^{3/2} \right] \right\}^{1/2}. \tag{2.5}$$

This describes the change in the radius of the slab with time after leaving a source of radius r_0. Using (2.3), we find the height of the slab to be

$$z(t) = \left\{ \left(\frac{r_0}{\beta}\right)^2 + \left(\frac{4}{3\beta\sqrt{\pi}}\right) \frac{M_0^{3/2}}{F_0} \left[1 - \left(1 - \frac{F_0 t}{M_0} \right)^{3/2} \right] \right\}^{1/2} - \frac{r_0}{\beta}. \tag{2.6}$$

The momentum flux is zero when the fountain reaches its maximum height. This occurs at time $T_0 \equiv M_0/F_0$. Substituting this into (2.6), the maximum height is

$$H_m \equiv z(T_0) = \left\{ \left(\frac{r_0}{\beta}\right)^2 + (\mathscr{C} H_0)^2 \right\}^{1/2} - \frac{r_0}{\beta}, \tag{2.7}$$

in which

$$H_0 \equiv {M_0}^{3/4} {F_0}^{-1/2} \tag{2.8}$$

is the characteristic fountain height based upon source parameters and

$$\mathscr{C} = \left[\frac{4}{3\beta\sqrt{\pi}} \right]^{1/2}. \tag{2.9}$$

For a fountain emanating from a point source, (2.7) reduces to the form originally obtained by Turner (1966) through dimensional analysis:

$$H_m \simeq \mathscr{C} H_0. \tag{2.10}$$

Using $\beta = 0.17$ as in Lee & Chu (2003), the proportionality constant is $\mathscr{C} \simeq 2.1$.

2.2. *Fountains in a uniform crossflow*

In the above discussion we have considered the rising fountain but have not gone on to examine the descending plume, which would interact with rising fluid. However, if the fountain rises in a sufficiently large horizontal crossflow, it can be bent over enough that the descending plume does not fall significantly upon the fluid emanating from the source, as illustrated in figure 1.

Here we classify the influence of the crossflow upon the fountain by the Froude number $Fr \equiv U_a/U_0$, which measures the ambient flow speed, U_a, relative to the characteristic fountain speed $U_0 = H_0/T_0 = F_0^{1/2} M_0^{-1/4}$. Our definition of Fr differs from the Froude number of Roberts & Toms (1987) by a factor $(\pi/4)^{1/4} \simeq 0.94$.

For relatively large ambient flows ($Fr \gg 1$), the relative horizontal momentum input at the source gives rise to counter-rotating vortices. Taking into account the resulting entrainment of ambient fluid, Chu (1975) predicted that the maximum height should scale as the Froude number according to $H_m/H_0 \simeq 1.60\, Fr^{-1/3}$. For moderate ambient flow speeds, only experimentally determined empirical predictions exist (e.g. Roberts & Toms 1987; Gungor & Roberts 2009). In particular, these authors found $H_m/H_0 \simeq 2.97$ for $0.21 < Fr < 0.85$ and $H_m/H_0 \simeq 2.82\, Fr^{-1/3}$ for $Fr > 0.85$.

Here we adapt the Lagrangian method to predict, among other quantities, the maximum height of fountains in a moderate crossflow. In the moving frame of

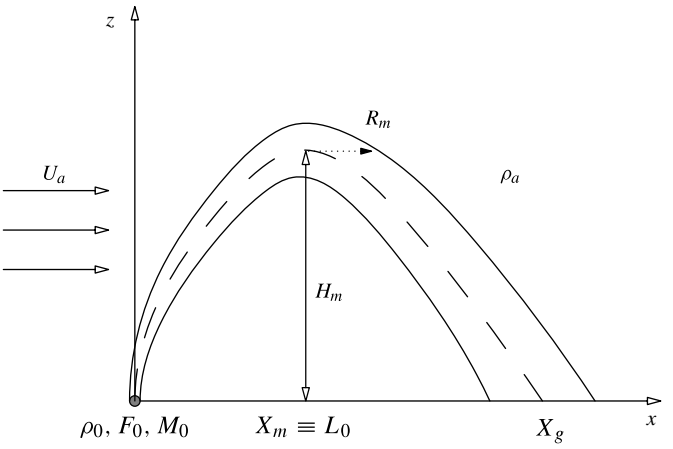

FIGURE 1. Schematic of a fountain in a uniform ambient with crossflow. At the maximum height, H_m, the fountain has radius R_m indicated by the dotted arrow. Note that the illustrated overshoot above H_m is not accounted for by the theory.

reference of the background crossflow for sufficiently small Froude numbers, the momentum flux at the source is predominantly vertical so we can neglect the development of streamwise vorticity. This assumption is corroborated by observations made during laboratory experiments.

For a slab of fluid leaving the source at time $t = 0$, its downstream distance from the source at time t as a result of being carried by the background crossflow is $x = U_a t$. Combining this with (2.6), the path of the ascending fluid is

$$z(x) = \left\{ \left(\frac{r_0}{\beta} \right)^2 + (\mathscr{C} H_0)^2 \left[1 - \left(1 - \frac{x}{L_0} \right)^{3/2} \right] \right\}^{1/2} - \frac{r_0}{\beta}, \tag{2.11}$$

in which $L_0 \equiv U_a T_0 = Fr H_0$.

As in a stationary ambient, the maximum height of the fountain is given by (2.7). Explicitly, assuming the source has negligibly small radius, the height is $H_m \simeq \mathscr{C} H_0 \simeq 2.1 H_0$. The last approximation, which assumes $\beta \simeq 0.17$ (Lee & Chu 2003), gives a proportionality constant, $\mathscr{C}$, moderately smaller than the value of 2.97 determined empirically by Roberts & Toms (1987). We attribute the discrepancy to the fact that the fluid leaving the source was not fully turbulent in their experiments.

In a crossflow the maximum height occurs downwind of the source at $x = L_0$. From (2.3), the corresponding radius at $z = H_m$ is

$$R_m \equiv \left[{r_0}^2 + (\beta \mathscr{C} H_0)^2 \right]^{1/2} = r_0 + \beta H_m \simeq \beta \mathscr{C} H_0, \tag{2.12}$$

in which the last approximation assumes a point source.

After reaching its maximum height the fountain falls downward as a plume. If the Froude number is sufficiently large that the plume does not fall back upon the source, the downflow regime of the fountain may be treated as a positively buoyant plume with initial conditions given by the parameters at the maximum height. Unlike a stationary fountain, a fountain in a moderate crossflow maintains its initial maximum height rather than reaching a smaller steady-state height, as a consequence of the descending fluid falling back upon the rising fluid from the source.

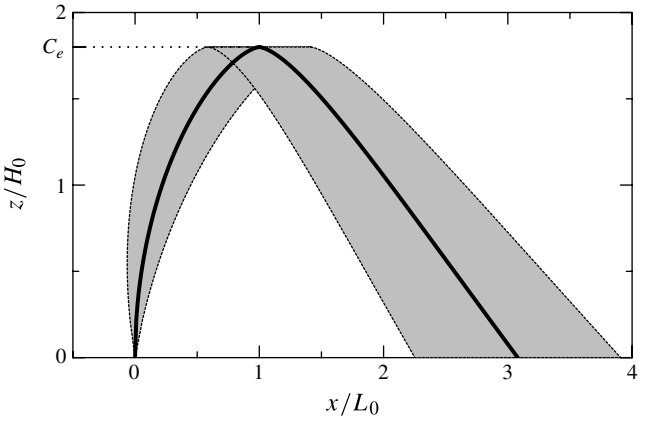

FIGURE 2. Plot of the centreline path (thick solid line) of a fountain in a uniform crossflow with $Fr = 1$ as predicted by Lagrangian theory via (2.11) and (2.14). The solution sets $\beta \equiv \beta_e = 0.23$ (hence $\mathscr{C} \equiv \mathscr{C}_e = 1.80$, as indicated) to be the empirical spreading parameter determined experimentally by (5.1). The grey-shaded region indicates the extent of the radial spreading $r(x)$ of the fountain.

Setting $\tau = t - T_0$ as the time governing the evolution of the descending plume which has zero momentum at $\tau = 0$, conservation of momentum requires $\mathrm{d}M/\mathrm{d}\tau = F_0$ and the change in radius of the descending plume is governed by $\mathrm{d}r/\mathrm{d}z = -\beta$.

As before, we manipulate these equations to get a differential equation for $r(\tau)$. Using $r = R_m$ at $\tau = 0$ and then writing the result in terms of the downstream distance $x = L_0 + U_a\tau$, the radius of the descending plume is

$$r(x) = \left\{ {R_m}^2 + (\beta\mathscr{C}H_0)^2 \left(\frac{x}{L_0} - 1\right)^{3/2} \right\}^{1/2}, \tag{2.13}$$

defined for $x \geqslant L_0$. The height of the descending centreline is

$$z(x) = H_m - \left\{ \left(\frac{R_m}{\beta}\right)^2 + (\mathscr{C}H_0)^2 \left(\frac{x}{L_0} - 1\right)^{3/2} \right\}^{1/2} + \frac{R_m}{\beta}. \tag{2.14}$$

The path of the fountain predicted by the Lagrangian theory is shown in figure 2. Note that the top of the fountain is flat and the radius (R_m) at the maximum height (H_m) is obtained from the fountain's horizontal extent at this height.

By putting $z = 0$ in (2.14), the horizontal distance, X_g, where the fountain impacts the ground can be determined. Substituting this in (2.13) gives the radius, R_g, at the point of impact. These quantities are simply expressed if we assume the source has negligibly small radius ($r_0 \ll \beta\mathscr{C}H_0$):

$$X_g = (1 + 3^{2/3})L_0 \simeq 3.08U_a\frac{M_0}{F_0} \quad \text{and} \quad R_g = \sqrt{2}\beta\mathscr{C}H_0 = (8\beta/3\sqrt{\pi})^{1/2}\frac{{M_0}^{3/4}}{{F_0}^{1/2}}. \tag{2.15}$$

The condition that the spreading core of the descending fountain does not significantly impact the source is $X_g > R_g$. For a point source, this condition imposes a

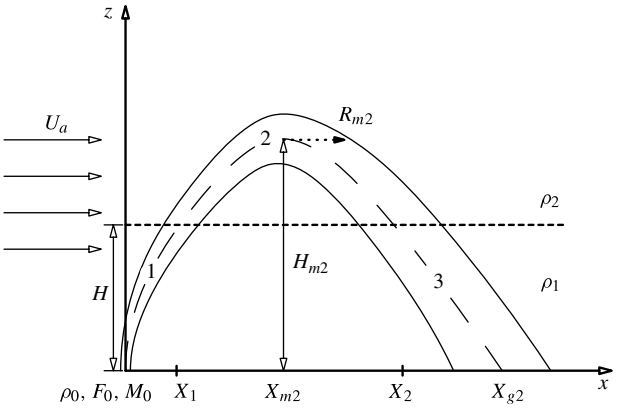

FIGURE 3. Schematic of a fountain in a two-layer fluid with uniform crossflow speed U_a. The regimes characterizing the fountain's evolution are labelled 1, 2 and 3. The interface between the upper and lower layers is indicated by the short-dashed line. The fountain is assumed to penetrate into the upper layer up to height H_{m2} where its radius is R_{m2}, indicated by the dotted arrow. Note that the theory does not account for the overshoot of the fountain above H_{m2}.

lower bound on the Froude number such that

$$Fr > \frac{1}{1+3^{2/3}}\left(\frac{8\beta}{3\sqrt{\pi}}\right)^{1/2}. \tag{2.16}$$

Using $\beta \simeq 0.17$ (Lee & Chu 2003) in the right-hand side of (2.16), the critical Froude number is 0.16. In § 5 we show that our experiments imply $\beta \equiv \beta_e \simeq 0.23$, in which case the critical Froude number is 0.19. (Note that here, as in the rest of the paper, experimentally measured quantities are denoted with subscript 'e'.) This lower bound is comparable to the value 0.21 obtained empirically by Roberts & Toms (1987).

Finally, we compute momentum and volume fluxes of the return flow at the level of the source to be

$$M_g = F_0\frac{X_g - L_0}{U_a} = M_0\left(\frac{X_g}{L_0} - 1\right) \quad \text{and} \quad Q_g = R_g\sqrt{\pi M_g}. \tag{2.17}$$

Note that $M_g \simeq 3^{2/3}M_0$ if the fountain is treated as a point source. This is more than double the momentum flux at the source due to the fact that the descent time of the fountain is more than twice the time taken to rise to its maximum height.

3. Theory for fountains in a two-layer ambient

Here we extend the theory presented in § 2 to the case of a fountain in a two-layer fluid with uniform crossflow. The lower layer has depth H and density ρ_1 and the upper layer is infinitely deep with density ρ_2. The speed of both layers relative to the source is U_a. To develop the theory, the path of the fountain is divided into three different regimes, as shown in figure 3.

Following the approach of Ansong *et al.* (2008), the fountain in regime 1 is treated like a fountain in a uniform ambient until it impinges on the density interface. We assume that the fountain penetrates substantially into the upper layer so that the fountain beyond the interface is treated like the one-layer case but with adjusted source conditions set by the fountain properties at the interface. From the fountain properties

in regime 1, the mean fluxes at the interface are calculated and these are used as source conditions for the rising fountain and descending plume in regime 2. Finally, we compute the fluxes associated with the descending plume impinging from above upon the interface. These are used to assess whether the plume continues to descend into regime 3 or whether the fluid remains trapped at the interface. Each of these steps are described explicitly below.

3.1. *Equations for regime* 1

In this regime the path of the fountain emanating from a source of radius r_0 is given by (2.11), valid for $0 \leqslant x \leqslant X_1$, in which X_1 is the horizontal position where the centreline of the fountain first impinges on the interface at $z = H$. Explicitly,

$$X_1 = L_0 \left[1 - \left\{ 1 - \frac{1}{(\mathscr{C}H_0)^2} \left[\left(H + \frac{r_0}{\beta} \right)^2 - \left(\frac{r_0}{\beta} \right)^2 \right] \right\}^{2/3} \right]. \tag{3.1}$$

Its radius at this height is

$$R_1 = r_0 + \beta H. \tag{3.2}$$

Using (2.1) and (2.4) with $x = U_a t$, we determine the momentum and volume fluxes at the interface to be

$$M_1 = M_0 - F_0 \frac{X_1}{U_a} = M_0 \left(1 - \frac{X_1}{L_0} \right), \tag{3.3}$$

$$Q_1 = R_1 \sqrt{\pi M_1}. \tag{3.4}$$

The buoyancy flux is constant while the fountain traverses the lower layer. Hence we determine the density of the fountain at the interface to be

$$\varrho_1 = \rho_1 + \rho_0 \frac{F_0}{g Q_1}. \tag{3.5}$$

3.2. *Equations for regime* 2

To track the movement of the fountain beyond the interface, we first calculate the buoyancy flux F_1 of the fountain above the interface. Using (3.5), this is given by

$$F_1 = Q_1 g (\varrho_1 - \rho_2)/\rho_0. \tag{3.6}$$

The path of the fountain above the interface is predicted by adapting (2.11) and (2.14) with source conditions established by the fountain radius R_1 and fluxes M_1 and F_1 at the interface. Up to its maximum height (for $X_1 < x \leqslant X_{m2}$), we find

$$z = H + \left\{ \left(\frac{R_1}{\beta} \right)^2 + (\mathscr{C}H_1)^2 \left[1 - \left(1 - \frac{x - X_1}{L_1} \right)^{3/2} \right] \right\}^{1/2} - \frac{R_1}{\beta}, \tag{3.7}$$

in which $H_1 = {M_1}^{3/4}/{F_1}^{1/2}$, $L_1 = U_a M_1/F_1$ and R_1 is given by (3.2). During its descent in the upper layer the path of the fountain is given by

$$z = H_{m2} - \left\{ \left(\frac{R_{m2}}{\beta} \right)^2 + (\mathscr{C}H_1)^2 \left(\frac{x - X_1}{L_1} - 1 \right)^{3/2} \right\}^{1/2} + \frac{R_{m2}}{\beta}, \tag{3.8}$$

which is valid for $X_{m2} \leqslant x \leqslant X_2$.

At $x = X_{m2} \equiv X_1 + L_1$, the fountain reaches its maximum height

$$H_{m2} = H + \left\{ \left(\frac{R_1}{\beta} \right)^2 + (\mathscr{C}H_1)^2 \right\}^{1/2} - \frac{R_1}{\beta} \simeq \left[H^2 + (\mathscr{C}H_1)^2 \right]^{1/2}, \tag{3.9}$$

in which the last approximation assumes a point source. The radius at this height is

$$R_{m2} \equiv R_1 + \beta(H_{m2} - H) = r_0 + \beta H_{m2}. \tag{3.10}$$

The horizontal location where the descending branch of the fountain impacts the interface is given by solving $z = H$ for x in (3.8). If we assume $r_0 \ll \beta\mathscr{C}H_0$, this occurs at

$$X_2 \simeq X_1 + L_1 \left[1 + \left\{ 3 + 4\delta^2 + 4\delta\sqrt{1+\delta^2} \right\}^{2/3} \right], \tag{3.11}$$

in which $\delta \equiv H/(\mathscr{C}H_1)$. This result shows that the fountain returns to the interface further downwind as the lower-layer depth becomes larger relative to $\mathscr{C}H_1$.

The plume radius at the interface is

$$R_2 \simeq R_1 + \sqrt{2}\beta(H_{m2} - H) \tag{3.12}$$

and the corresponding momentum and volume fluxes are

$$M_2 = F_1 \frac{X_2 - X_m}{U_a} = M_1 \frac{X_2 - X_m}{L_1} \quad \text{and} \quad Q_2 = R_2\sqrt{\pi M_2}. \tag{3.13}$$

Finally, we compute the density of the fountain at the interface to be

$$\varrho_2 = \rho_2 + \rho_0 \frac{F_1}{gQ_2}. \tag{3.14}$$

Depending upon the buoyancy of the plume relative to the lower-layer fluid, the fountain may fall to the ground, get trapped at the interface or exhibit both regimes. Similar to the approach of Briggs (1969) (see also Briggs 1975; Manins 1979; Weil 1988), we expect the descending flow to propagate through the bottom layer if $\varrho_2 > \rho_1$ and is trapped at the interface if $\varrho_2 < \rho_1$. In reality, due to inhomogeneities in the density across the slab of fluid at the interface in experiments we expect both regimes will occur if $\varrho_2 \simeq \rho_1$. The condition that $\varrho_2 < \rho_1$ for interface-spreading also provides a succinct expression relating the density ratios to the ratios of the volume fluxes in the problem: $[(\rho_0 - \rho_1)/(\rho_1 - \rho_2)] < (Q_2/Q_0)[1 - (Q_1/Q_2)]$. These criteria will be examined in § 5.

Another approach that may be used to classify the regimes of flow is the method used in the case of fountains in two-layer stationary environments (Ansong *et al.* 2008). The most significant factors governing the flow regimes are the relative density differences between the two layers and fountain and the potential maximum height that would be reached passing through the lower layer relative to the actual depth, H, of this layer. Explicitly, the relative maximum height is characterized by H_m/H, in which H_m is given by (2.7). If the radius of the source is sufficiently small, the relative height is just $\mathscr{C}H_0/H$. The relative density differences are characterized by

$$\theta = \left| \frac{\rho_1 - \rho_2}{\rho_0 - \rho_2} \right|. \tag{3.15}$$

This is defined so that $\theta = 0$ if $\rho_2 = \rho_1$, in which case the ambient is a one-layer fluid and the fountain must return to the level of the source, and $\theta = 1$ if $\rho_0 = \rho_1$, in which

case the source has the same density as the lower-layer fluid and so emanates as a jet. In the former case the fountain must return to the ground. In the latter case the jet impinging above the interface entrains less dense fluid and so becomes lighter than the ambient fluid at the source. Hence the descending flow will spread along the interface instead of the ground.

3.3. *Equations for regime 3*

In considering the flow in this last regime we suppose the descending plume has enough buoyancy to penetrate beyond the interface and reach the ground. Using ϱ_2 from (3.14), the buoyancy flux of the descending plume below the interface is

$$F_2 = Q_2 g(\varrho_2 - \rho_1)/\rho_0. \tag{3.16}$$

The source momentum and volume fluxes are given by (3.13) and the source radius is given by (3.12).

The centreline of the plume follows the path given by

$$z(x) = H - \left\{ \left(\frac{R_2}{\beta}\right)^2 + (\mathscr{C}H_2)^2 \left[\left(1 + \frac{x - X_2}{L_2}\right)^{3/2} - 1 \right] \right\}^{1/2} + \left(\frac{R_2}{\beta}\right), \tag{3.17}$$

for $X_2 \leqslant x \leqslant X_g$. Here $H_2 = M_2^{3/4}/F_2^{1/2}$ and $L_2 = U_a M_2/F_2$.

The plume contacts the ground at

$$X_g = X_2 + L_2 \left[\left\{ \frac{(H + R_2/\beta)^2 - (R_2/\beta)^2}{(\mathscr{C}H_2)^2} + 1 \right\}^{2/3} - 1 \right]. \tag{3.18}$$

The radius at the ground is

$$R_g = \left\{ {R_2}^2 + (\beta\mathscr{C}H_2)^2 \left(\left[\frac{x - X_2}{L_2} + 1 \right]^{3/2} - 1 \right) \right\}^{1/2} \tag{3.19}$$

and the momentum flux, M_g, and volume flux, Q_g, at the point of impact are

$$M_g = M_2 + F_2 \frac{X_g - X_2}{U_a} = M_2 \left(1 + \frac{X_g - X_2}{L_2}\right) \quad \text{and} \quad Q_g = R_g \sqrt{\pi M_g}. \tag{3.20}$$

In the absence of a crossflow, fountains are often classified as 'forced', 'weak' or 'very weak' based upon the value of the source Froude number $Fr_0 = w_0/\sqrt{(r_0 g_0')}$. The particular regime of flow gives information on whether or not the steady-state height of the fountain depends linearly upon the source Froude number. The study by Kaye & Hunt (2006) concluded that the transition from highly forced to weak fountains appears to occur at $Fr_0 \approx 3$, while the transition from weak to very weak fountains depends on both the Froude number and Reynolds number of the flow. The model above was applied to experiments in which the fountain was 'forced' at the source ($6 < Fr_0 < 21$) and moderately 'forced' at the interface ($1.5 < Fr_i < 7.6$). Here Fr_i is the Froude number at the interface, defined like Fr_0 but with source parameters replaced by those at the interface.

4. Experimental set-up and analyses

4.1. *Experimental set-up*

Most experiments were performed in an acrylic tank with inner dimensions 50 cm × 50 cm × 50 cm, with some being conducted in a tank measuring 39.5 cm ×

39.5 cm × 39.5 cm. Here we describe the experimental set-up and procedure for the larger tank though a similar procedure was used for the smaller tank. A total of 74 experiments were conducted: 14 in uniform (one-layer) ambients and 60 in two-layer ambients.

The total depth of fluid within the tank was $H_T = 48$ cm. The variations in density were created using sodium chloride solutions, and density samples were measured using the Anton Paar DMA 4500 density meter. In two-layer experiments the upper layer depth was either $H = 3$ or 5 cm with typical interface thicknesses of 0.5 cm. All experiments were conducted by injecting fresh water downward into a more dense saline ambient. Because the system is Boussinesq the results are dynamically equivalent to injecting heavy fluid upward from the bottom.

A reservoir of blue-dyed fresh water of density ρ_0 was injected into the tank by a Monostat peristaltic pump. The flow rates for the experiments, recorded by measuring the total volume released during an experiment, ranged from 0.95 to 2.73 cm^3 s^{-1}. The flow was injected through a $r_0 = 0.2$ cm radius nozzle fitted with a fine mesh having openings of 0.05 cm to ensure the flow was turbulent at the source. The Reynolds number of the experiments, defined as $R_e = w_0 D_0/\nu$, ranged from 300 to 865, where ν is the kinematic viscosity of water and $D_0 = 2r_0$.

A crossflow was simulated by connecting the nozzle to a horizontal traverse that moved at speeds ranging between 0.11 and 0.85 cm s^{-1}. To avoid downwash effects, the nozzle was usually placed just a few millimetres (∼0.3 cm) into the top-layer fluid. There was negligible disturbance to the top-layer fluid as a result of the horizontal movement of the nozzle except for small capillary waves.

The experiments were recorded using a Sony DCR-TRV6 digital camera situated 300 cm from the front of the tank. The camera was situated at a level parallel to the upper mid-depth of the tank and the entire tank was in its field of view. Fluorescent lighting was placed 10 cm behind the tank to illuminate the set-up. In a few experiments, a second camera was placed above the tank and looking down on the tank surface at an angle of 45° from the horizontal.

The experiments were analysed using the Image Processing Toolbox in MATLAB. These analysis methods are described below.

4.2. *Qualitative analyses*

Although the experiments were performed with source fluid being injected downwards, for ease of comparison with theory and the atmospheric application in question we present snapshots of experiments flipped upside-down so that it appears as if the fluid is injected upwards. Correspondingly, we refer to the motion of the fluid from the source as being 'upward' and of the return flow being 'downward'. Also the fountain source was towed through a stationary ambient. However, using the language of a crossflow over a stationary source, we refer to the horizontal motion of the gravity currents at the 'ground' moving toward the source as 'upstream' and moving away from the source as 'downstream'.

4.2.1. *One-layer experiments*

Figure 4 shows snapshots of a fountain in a one-layer crossflow at six different times after the injection of dyed fluid started at $t = 0$. In these images, the initial background image was subtracted to accentuate intensity differences due to the dyed fountain. In the experiments fresh water was injected with a volume flux of $Q_0 = 2.73$ cm^3 s^{-1} into a salt water ambient of density $\rho_1 = 1.0037$ g cm^{-3}. Dividing by the area of the nozzle $\pi r_0^2 = 0.126$ cm^2, the initial velocity was $w_0 = 21.7$ cm s^{-1}.

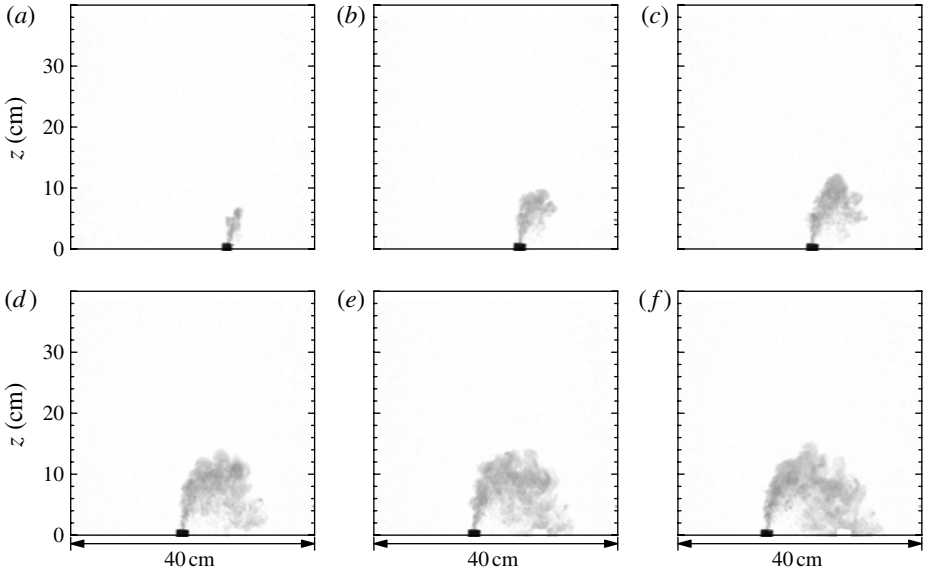

FIGURE 4. Snapshots with background subtracted of a fountain in a one-layer crossflow at the six times indicated after the fluid is first injected at $t = 0$. Experimental parameters are $Q_0 = 2.73$ cm^3 s^{-1}, $|\rho_0 - \rho_1| = 0.0055$ g cm^{-3} and $U_a = 0.85$ cm s^{-1}. The corresponding Froude number is $Fr = 0.61$ and characteristic horizontal and vertical length scales are $L_0 = 3.44$ cm, and $H_0 = 5.58$ cm: (*a*) $t = 2$ s; (*b*) $t = 4$ s; (*c*) $t = 6$ s; (*d*) $t = 10$ s; (*e*) $t = 12$ s; (*f*) $t = 14$ s.

From these parameters we compute the momentum flux at the source to be $M_0 = 59.2$ cm^4 s^{-2} and the buoyancy flux is $F_0 = 14.7$ cm^4 s^{-3}. Hence the characteristic height and time scales are $H_0 = {M_0}^{3/4}/{F_0}^{1/2} = 5.6$ cm and $T_0 = M_0/F_0 = 4.0$ s, respectively.

The source moved from right to left at a speed of $U_a = 0.85$ cm s^{-1}. From this we compute the characteristic horizontal length scale to be $L_0 = U_a T_0 = 3.4$ cm. The Froude number is $Fr = U_a/(H_0/T_0) = 0.61$.

Consistent with the moderate value of the Froude number, there was negligible interaction between the ascending and descending flows. The snapshots show the characteristic widening of the fountain as it entrained fluid from the surrounding homogeneous ambient and travelled mainly upward due to its initial momentum (figure 4*a,b*). The fountain reached its maximum height at $t \sim 6$ s (figure 4*c*). The fountain descended as a positively buoyant plume in the lee of the source at $t \sim 10$ s (figure 4*d*) and reached the ground at $t \sim 12$ s (figure 4*e*). Afterward the dyed fluid at the ground spread horizontally outward while the fountain itself could be considered to evolve in a statistically steady state.

In this experiment, the fountain fell almost directly upon the original position of the source. This is apparent as the 'ghost-image' of the original nozzle's position which whites out the plume after the initial image has been subtracted (figure 4*f*). This demonstrates that the horizontal momentum flux associated with the towed source is negligible compared with the vertical momentum flux: except for horizontal motion associated with mixing, injected fluid parcels effectively leave the source and move vertically up then down, returning approximately to the location from which they were injected. Consistent with theory and the observations of Gungor & Roberts (2009), the

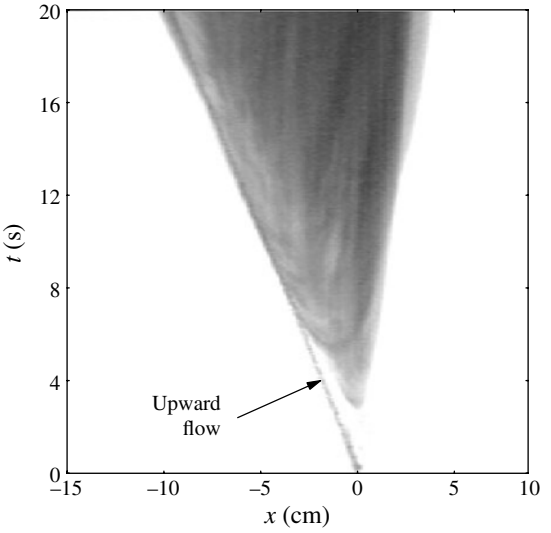

FIGURE 5. Horizontal time series taken at $z = 0$ and showing the downstream and upstream advance of gravity currents that result from a fountain in a one-layer crossflow with $U_a = 0.64$ cm s^{-1} ($Fr = 0.48$). The fluid emanating from the source is indicated with an arrow.

ascending fountain followed a steep trajectory whereas the return flow descended with a shallower slope.

Once the fountain impacted the ground, it spread in different directions. Unlike fountains in stationary environments in which the descending flow spread radially about the source (Ansong *et al.* 2008), these gravity currents were not axisymmetric and showed more complicated behaviour.

To examine the advance of the gravity currents, we constructed horizontal time series at the level of the source as shown in figure 5. The time series captured the gravity currents propagating upstream and downstream as well as the horizontal translation of the fluid emanating from the source. In this experiment, with $H_0 = 2.0$ cm and $Fr = 0.48$, the fountain first returned to the ground at $t \sim 3$ s. The upstream currents caught up with the source flow at $t \sim 7$ s and thereafter advanced in the laboratory frame at approximately the same speed as the towed source. In the source frame, the upstream gravity current was nearly stationary. Gungor & Roberts (2009) observed that the (source-relative) upstream flow ceased for values of Fr between 0.25 and 0.39, a range moderately smaller than the Froude number of the experiment shown in figure 5. The downstream currents propagated at almost constant speed away from the source.

4.2.2. *Two-layer experiments*

In the presence of a two-layer environment, the descending flow of a fountain may go back to the level of the source or it may mix sufficiently with the second layer so that it returns just to the interface. In some circumstances, it may do both. In this two-layer experiment the ratio of the source volume flux to the volume flux at the interface (Q_0/Q_1) lies between 0.16 and 0.30.

Figure 6 shows snapshots of a fountain in a two-layer fluid taken at six different times after the start of an experiment. At the interface, situated $H = 5$ cm above the source, the density jumps by $|\rho_1 - \rho_2| = 0.0018$ g cm^{-3}. The fluid is

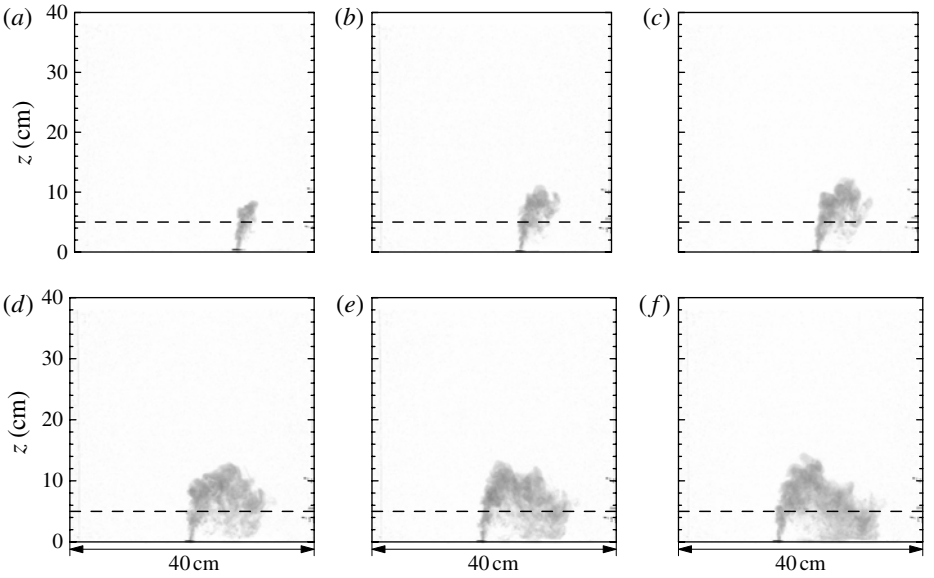

FIGURE 6. Snapshots at the times indicated of a fountain in a two-layer crossflow with the fountain returning to the ground. The horizontal dashed line indicates the height of the interface. Experimental parameters are $Q_0 = 2.7$ cm^3 s^{-1}, $|\rho_0 - \rho_1| = 0.0029$ g cm^{-3}, $|\rho_0 - \rho_2| = 0.0047$ g cm^{-3}, $H = 5$ cm and $U_a = 0.85$ cm s^{-1}. Other related parameters are $Fr = 0.85$, $L_0 = 6.4$ cm and $H_0 = 8.2$ cm: (*a*) $t = 2$ s; (*b*) $t = 4$ s; (*c*) $t = 6$ s; (*d*) $t = 10$ s; (*e*) $t = 12$ s; (*f*) $t = 14$ s.

injected at the source with momentum and buoyancy fluxes $M_0 = 60.8$ cm^4 s^{-2} and $F_0 = 7.67$ cm^4 s^{-3}, respectively. The corresponding characteristic height of the fountain is $H_0 = 7.9$ cm, implying that the fountain should penetrate into the upper layer. Indeed this is evident in the images which show the fluid passing into the upper layer without noticeable change in structure (figure 6*a,b*). The fountain reached the maximum height at $t \sim 6$ s (figure 6*c*) and then descended back through the interface, returning ultimately to the ground (figure 6*d–f*).

In contrast, figure 7 shows snapshots of a two-layer experiment in which the returning flow became trapped at the interface. Although the tow speed, source volume flux and lower-layer depth are the same as the experiment shown in figure 6, the primary difference here is that the density jump between the lower- and upper-layer fluids is greater. Here $|\rho_1 - \rho_2| = 0.0038$ g cm^{-3}. In comparison with the previous case, after penetrating into the upper layer the fountain entrains relatively less dense fluid, making the fountain itself less dense. The dilution of the fountain is sufficient to make it buoyant relative to the lower layer when it returns to the interface. Figure 7(*d*) shows that the descending fluid reached the interface and overshot it due to its momentum. At subsequent times (figure 7*e,f*) the descending fluid continued to overshoot the interface and rose back to spread horizontally around the interface. This behaviour is similar to what was observed in fountains in two-layer stationary environments, although in that case the spreading layer was symmetric about the central core of the fountain (Ansong *et al.* 2008).

Similar to the one-layer experiments, horizontal time series (not shown) of gravity currents intruding on the interface or propagating along the ground were observed to spread initially at a constant speed.

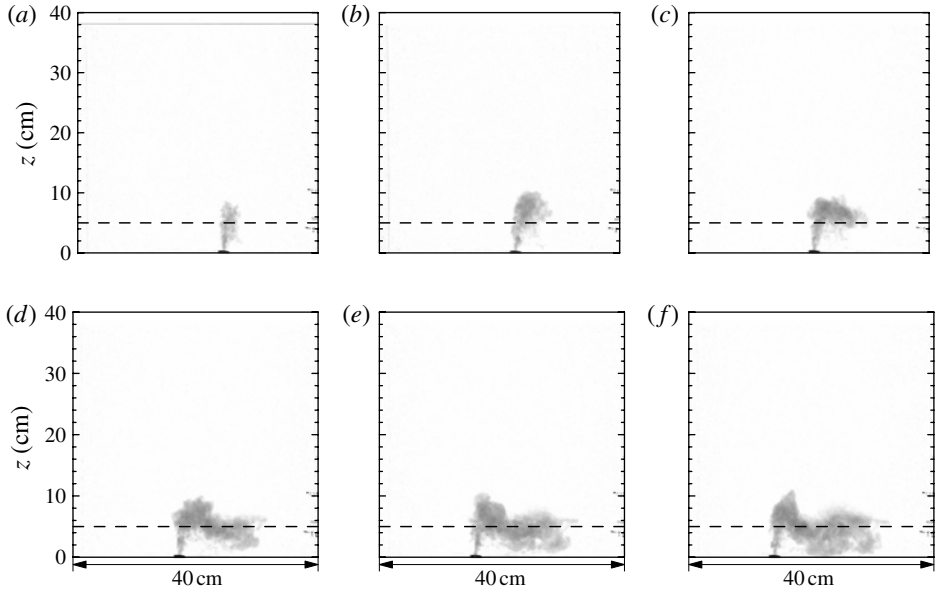

FIGURE 7. As in figure 6 but showing snapshots of a fountain in a two-layer crossflow with the fountain returning to the interface alone. Experimental parameters are $Q_0 = 2.7$ cm^3 s^{-1}, $|\rho_0 - \rho_1| = 0.0025$ g cm^{-3}, $|\rho_0 - \rho_2| = 0.0062$ g cm^{-3}, $H = 5$ cm and $U_a = 0.85$ cm s^{-1}. Other related parameters are $Fr = 0.91$, $L_0 = 7.5$ cm and $H_0 = 8.2$ cm: (*a*) $t = 2$ s; (*b*) $t = 4$ s; (*c*) $t = 6$ s; (*d*) $t = 10$ s; (*e*) $t = 12$ s; (*f*) $t = 14$ s.

5. Results and comparison with theory

Here we present the experimental results and compare them with one-layer and two-layer theory. The one-layer experiments are used to determine the empirical parameter β, which denotes the relative spreading rate of the plume. As well as to quantify the maximum penetration height of fountains in one- and two-layer crossflows and characterize the various regimes of flow that occur when fountains evolve in two-layer ambients.

5.1. *One-layer experiments*

To compare the path of the fountain with theory, we first constructed the average of a sequence of snapshots, each shifted horizontally so that the source was situated at the same location. Averaging was performed over 5 s beginning from the time when the fountain first returned to the level of the source. Figure 8(*a*) shows the corresponding averaged image for the experiment shown in figure 4. Superimposed on this image we have overlaid the theoretical path given by (2.11) and (2.14). The theory satisfactorily shows the steep rise to the maximum height and the gradual descent back to the ground.

Constructing the theoretical curve first required the empirical determination of the spreading parameter β. To do this we measured the maximum height of fountains in a one-layer fluid with crossflow for a range of experiments with varying Q_0, $|\rho_0 - \rho_1|$ and U_a. The results are shown in figure 9(*a*), which plots the measured values of the maximum height H_{me} against the characteristic height H_0 determined from experimental parameters using (2.8). A best-fit line through the data gives a

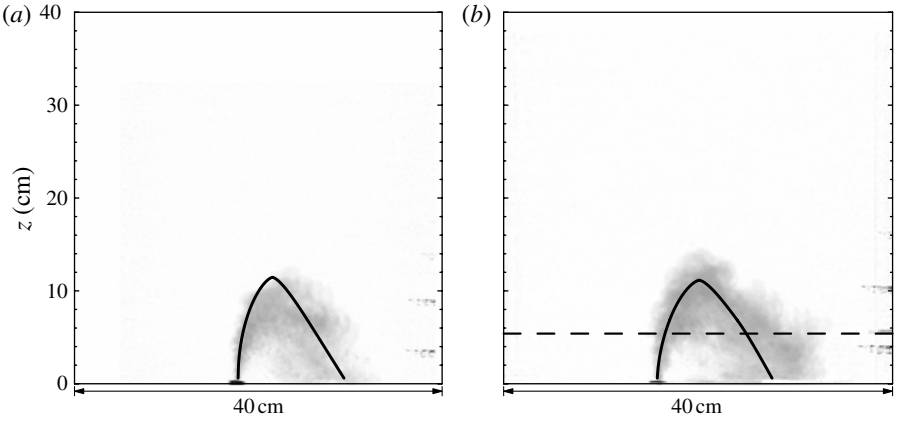

FIGURE 8. Shifted and averaged images with superimposed path predicted by theory for a fountain in (*a*) a one-layer fluid and (*b*) a two-layer fluid. The experimental parameters for (*a*) and (*b*) are the same as for those in figures 4 and 6, respectively.

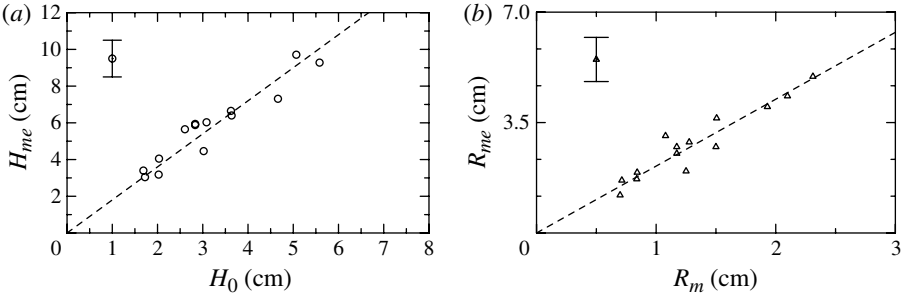

FIGURE 9. (*a*) The measured maximum height H_{me} plotted against the characteristic height H_0, and (*b*) the measured radius at the maximum height R_{me} versus the radius R_m predicted by (2.12) for fountains in a one-layer crossflow. The typical errors in measurements are indicated in the top-left corner of each plot.

relationship of the form

$$H_{me} = (1.80 \pm 0.05)H_0. \tag{5.1}$$

Using (2.9) and the point-source approximation in (2.10), we thus determine the spreading parameter to be $\beta \equiv \beta_e \simeq 0.23 \pm 0.05$. This is greater than the value 0.17 obtained in the case of stationary fountains (Lee & Chu 2003). The difference is attributed in part to the turbulent nozzle we used and also to our indirect method of finding β from H_m. Although our comparison assumed a point source of flow, it did not significantly affect our results because the source radius was only a few per cent of the typical maximum heights measured. Following Morton (1959), we calculated the virtual origin from the source fluxes and found it to be around 1.0 cm.

The corresponding value of $H_{m0}/H_0 \simeq H_{me}/H_0 \equiv \mathscr{C}_e = 1.80$ is lower than the value 2.97 obtained by Gungor & Roberts (2009). The discrepancy is attributed to the fact that the nozzle in their experiments was not fitted with any mesh to trigger turbulence at the source and so the fountain entrained less ambient fluid near the source (Morton 1959), retarding its spreading with height.

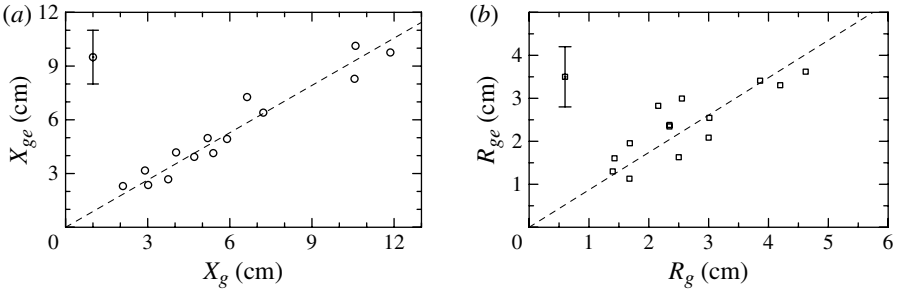

FIGURE 10. (*a*) The measured horizontal distance of the impact point X_{ge} versus the theoretical value X_g, and (*b*) the measured radius at the impact point R_{ge} versus the theoretical value R_g, of fountains in one-layer crossflows. The typical error bars are indicated in the upper left-hand corner of each plot.

The dilution of the fountain at the maximum height is determined by its radius, R_m (Chu 1975; Middleton 1986). For a range of experiments we measured the radius at the maximum height R_{me}. These are compared with the theoretical value given by (2.12) in figure 9(*b*). The plot shows a relationship of the form

$$R_{me} = (2.12 \pm 0.06)R_m. \tag{5.2}$$

The measured values are consistently higher than predicted. We attribute the discrepancy to interactions between the rising and descending branches of the fountain, which overlap near its top. Although not apparently affecting the path of the fluid in the fountain, the interaction causes the rising fluid to entrain into the descending flow, resulting in a relatively larger width at the maximum height. Moreover, the vertical position of the centreline at the maximum height is difficult to locate as a result of the merging of the upward–downward flows.

Next we focus on the properties of the fountain where it impacted the ground. The horizontal distance from the source, X_{ge}, where the centreline of the fountain reaches the ground, was measured as the central location where fluid from the fountain contacted the ground and begins to spread out. Figure 10(*a*) compares this with the theoretical value X_g given by (2.15). The best-fit line through data determined in a range of experiments reveals a relationship of the form

$$X_{ge} = (0.88 \pm 0.03)X_g. \tag{5.3}$$

That the theory moderately overestimates the measured value is attributed to the fact that the theory neglects interactions between the upward and downward branches of the fountain near its maximum height. By entraining part of the rising fluid, the descending plume is moderately more dense than theory predicts.

The relationship between the measured average radius of the fountain, R_{ge}, at the impingement point and the theoretical relation in (2.15) is shown in figure 10(*b*). In these one-layer experiments, the measured radii at the point of impact are the averages of two independent measurements, one from the side-view camera and the other from a second camera looking down on the tank surface at an angle of 45°. The data show a relation of the form

$$R_{ge} = (0.87 \pm 0.13)R_g. \tag{5.4}$$

The scatter in this plot is due, in part, to the difficulty in accurately measuring the width of the fountain after impact: once the fountain impacts the ground, it

immediately begins to spread outward in all directions. A second reason is the shape of the fountain at the point of impact. The shape is not completely circular as the theory assumes.

In most experiments horizontal time series show that the currents spread at a constant speed in the downstream direction after the fountain impacted the ground. This result is consistent with the theory first proposed by Kotsovinos (2000), and with observations by Ansong *et al.* (2008) of fountains in stationary ambients and by Ansong & Sutherland (2010) of buoyant plumes in a uniformly stratified environment. Upstream currents were not measured because of difficulty in distinguishing their fronts from the upward flow of the fountain.

Although we measured the speed of these currents, unlike the results of a stationary fountain (Ansong *et al.* 2008) we found no correlation between the measured speeds and the characteristic speed based upon the fluxes M_g and Q_g at the ground. Likewise there was no obvious correlation between the measured speeds and U_a.

5.2. *Two-layer experiments*

Figure 8(*b*) shows the shifted and averaged image of snapshots taken from the experiment shown in figure 6. Upon this image, we have overlaid the theoretical path in the three regions described in § 3 given by (2.11), (3.7), (3.8) and (3.17). In applying this theory, we used the value $\beta = \beta_e = 0.23$, determined from the one-layer experiments. The comparison shows that the theory satisfactorily describes the path of the fountain.

5.2.1. *Return-flow spreading characterization*

Three types of spreading flow were observed in the experiments: 'ground-spreading', 'interface-spreading' and 'dual-spreading'. The first refers to the case in which the descending flow penetrates the interface and returns to the level of the source. The second refers to the case in which the return flow is trapped at the interface. In the last case, both circumstances occur. Cases in which the rising fountain impacts the density interface without penetration were not investigated in this study.

To predict the type of spreading, we compared ϱ_2, given by (3.14) to the lower layer density, ρ_1. The descending flow is expected to penetrate the interface if $\varrho_2 > \rho_1$, in which case the fountain should become ground-spreading. If $\varrho_2 < \rho_2$, the fountain should be interface-spreading. (Of course, these theoretical criteria are posed for a fountain initially injected upward; in our experiments, for which the fountain is injected downward, the conditions are reversed. In the discussion that follows, however, we continue to use the language appropriate for upward-injected fountains.) Dual-spreading is expected if $\varrho_2 \simeq \rho_1$.

In the case of ground-spreading fountains, the prediction of theory is good if $(\varrho_2 - \rho_1)/\rho_0 \gtrsim 0.0001$ while interface trapping is well predicted if $(\varrho_2 - \rho_1)/\rho_0 \lesssim 0.0002$. However in experiments in which dual-spreading was observed, there were large variations in the relative density difference within the range $|\varrho_2 - \rho_1|/\rho_0 \lesssim 0.002$. In many of the dual-spreading experiments the spreading flow was observed to be primarily interface-spreading but with some fluid raining out of the intrusion eventually spreading at the ground. Typically this results because the horizontal density profile across the descending plume is not in fact uniform: the outer part of the descending flow is less dense than the core. For dual-spreading currents the extremities of the plume become trapped at the interface while the fluid near the core eventually descends to the ground.

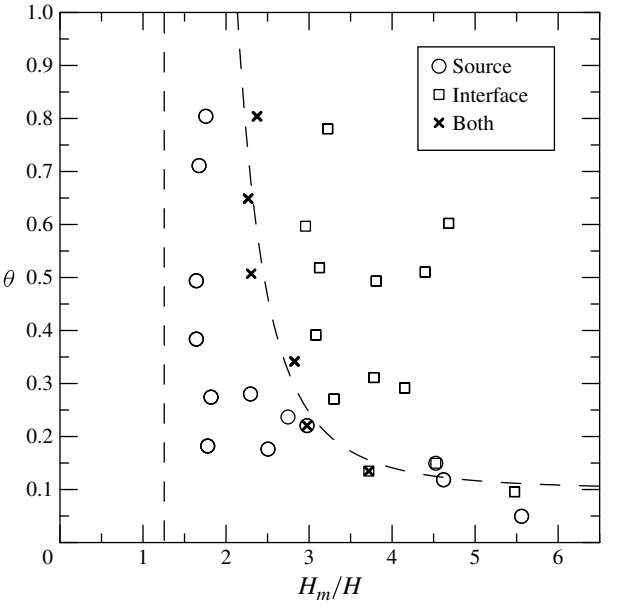

FIGURE 11. Regime diagram showing the circumstances under which the return flow of a fountain spreads at the level of the source (open circles), at the interface (open squares), or both. The dashed line represents an empirical formula that separates the two regimes and is given by (5.5).

We found that the distinction between ground-spreading and interface-spreading regimes, though less rigorous on physical grounds, could conveniently be characterized by two parameters: the relative density difference $\theta \equiv (\rho_1 - \rho_2)/(\rho_0 - \rho_2)$ (see (3.15) and the discussion below), and the predicted maximum height relative to the lower layer depth, H_m/H, in which H_m is given by (2.10). Both parameters are readily determined from the source conditions. The corresponding spreading-regime diagram is plotted in figure 11. The diagram clearly shows separation in parameter space between the ground-spreading and interface-spreading flows. The boundary separating the regimes is given approximately by the empirical function

$$\theta = 0.1 + \frac{1}{(H_m/H - 1.1)^3}, \tag{5.5}$$

and is plotted as the dashed line in figure 11. If $\theta > 0.1$, we find intrusions form if $H_m \gtrsim 2H$ to $3H$. In this case, the fountain penetrates sufficiently deep into the upper layer that the rising and descending fluid entrains the sufficiently less dense fluid to be buoyant when the fountain returns to the interface. If $H_m \lesssim 2H$ the descending flow is found to return to the ground irrespective of the value of θ.

For any value of H_m/H, the fountain returned to the ground if $\theta < 0.1$. This occurred either because the fountain did not penetrate significantly into the upper layer, in which case there was little mixing with this less dense fluid, or because the density difference between the two layers was so small, in which case the ambient acted effectively as a one-layer fluid.

Qualitatively similar behaviour was observed in the case of a two-layer fountain with no crossflow (Ansong *et al.* 2008). In that study the fountain returned to the ground for any H_m/H if $\theta < 0.15$. By reducing mixing between the rising and falling

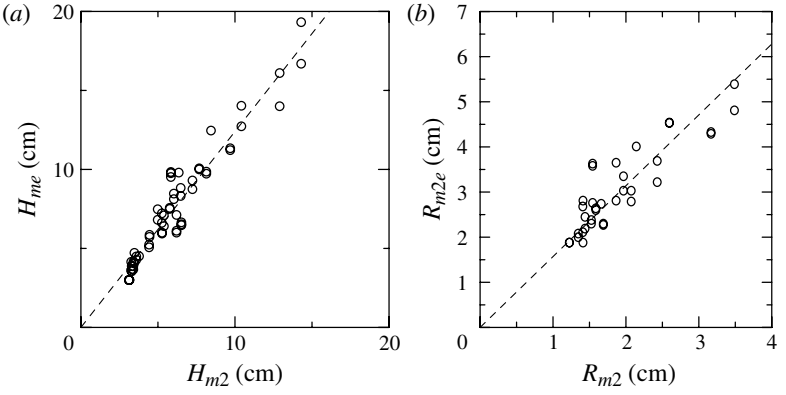

FIGURE 12. (*a*) The measured maximum height H_{me} plotted against the predicted height H_{m2}, and (*b*) the measured radius at the maximum height R_{m2e} versus the radius R_{m2} predicted by (3.10) for fountains in a two-layer crossflow. The best-fit line through each data set is indicated by the dashed line.

fluid in a fountain, a moderate crossflow acts to lower this threshold, though not significantly. Due to the development of streamwise vorticity and consequent enhanced entrainment in a strong crossflow, the threshold is expected to lower further, though this has not been examined in our experiments.

5.2.2. *Maximum height*

As in the one-layer experiments, we measured the maximum height, H_{me}, as the top of the fountain determined from averaged and shifted snapshots of the experiment as shown in figure 8(*b*). In figure 12(*a*), these are plotted against the height, H_{m2}, predicted by (3.9) using the values $\beta = \beta_e$ and $\mathscr{C} = \mathscr{C}_e$ determined from our one-layer experiments. The best-fit line through the data gives the relationship

$$H_{me} = (1.24 \pm 0.04)H_{m2}. \tag{5.6}$$

The two-layer theory underpredicts the maximum height by about 25 %, which is some indication of the errors associated with determining β_e through the maximum height of a one-layer fountain.

Figure 12(*b*) plots the radius at the maximum height against the radius, R_{m2}, predicted by (3.10). The best-fit line through the data gives

$$R_{m2e} = (1.57 \pm 0.13)R_{m2}, \tag{5.7}$$

and shows, similar to the one-layer case, that the theory underestimates the radius at the maximum height. Note that figure 12(*b*) and all other figures in the rest of the paper were plotted for experiments in which the lower edge of the fountain at the maximum height clearly penetrated the interface.

5.2.3. *Impact position and radius*

We measured the horizontal position where the downflow impinged on the density interface (for fountains that exhibited interface and dual regimes) or the ground. Measurements were taken only from experiments in which there was substantial penetration into the upper layer. Figure 13 compares the result with theoretical predictions given by (3.11) and (3.18). The best-fit line through the data gives

$$X_{2e} = (1.07 \pm 0.11)X_2, \tag{5.8}$$

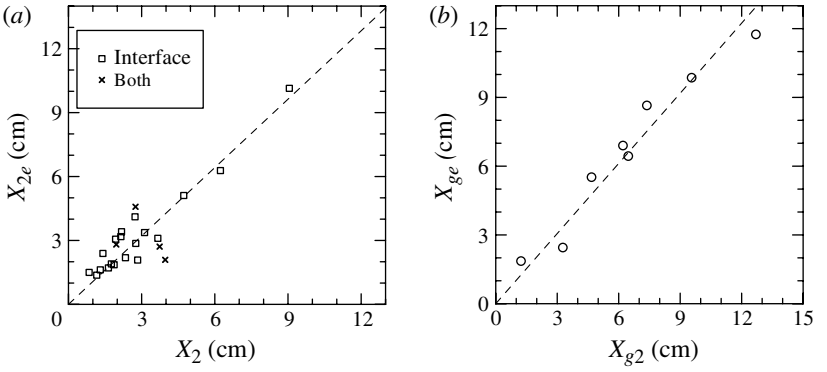

FIGURE 13. Experiments of two-layer fountains showing (*a*) the measured horizontal position of the point where the fountain impacts the interface, X_{2e}, versus the theoretical value, X_2 (3.11), for fountains trapped at the interface or exhibiting both regimes, and (*b*) the measured horizontal position where the fountain impacts the ground, X_{ge}, versus the theoretical value, X_{2g} (3.18). The best-fit line through the data is indicated by the dashed line.

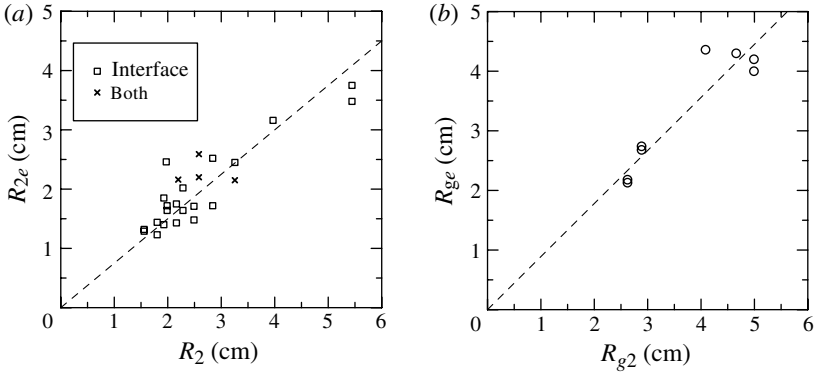

FIGURE 14. Experiments of fountains in a two-layer crossflow showing (*a*) the measured radius at the point where the fountain impacts the interface, R_{2e}, versus the theoretical value, R_2 (3.12), for fountains trapped at the interface or exhibiting both regimes, and (*b*) the measured radius at the point where the fountain impacts the ground, R_{ge}, versus the theoretical value, R_g (3.19).

$$X_{ge} = (1.02 \pm 0.03)X_g. \tag{5.9}$$

The radius of the downflow at the density interface (for fountains that exhibited interface and dual regimes) or the ground were also measured. Figure 14 plots these results. The predicted relations given by (3.12) and (3.19) are compared respectively to the observed values, R_{2e} and R_{ge}, to get

$$R_{2e} = (0.75 \pm 0.16)R_2, \tag{5.10}$$

$$R_{ge} = (0.89 \pm 0.01)R_{2g}. \tag{5.11}$$

6. Summary and conclusions

We have extended the Lagrangian theory for fountains in stagnant environments to the case of fountains in one and two layers with moderate crossflows characterized by Froude numbers between 0.4 and 0.8. Unlike stationary fountains in a one-layer fluid, because a fountain in a moderate crossflow falls negligibly back upon itself the steady-state height equals the initial maximum height. This measured height is consistent with measurements of the maximum height of stationary fountains (Turner 1966, e.g.).

From experiments on turbulent fountains in one-layer crossflows, we determined the value of the empirical spreading constant $\beta \simeq 0.23$. In general, there was good agreement between theory and experiment for these one-layer experiments. In particular, the path and the horizontal position of the point of impact were well determined.

The model could easily be refined by incorporating a different spreading coefficient for the returning plume. However, because the values of β for plumes in a crossflow range widely (between 0.34 and 0.62: Lee & Chu 2003), we chose a single spreading coefficient to keep the interpretation of our results conceptually easier.

Using the value of β determined from the one-layer experiments in the theory for two-layer fountains in a crossflow, we found that the maximum height was underpredicted by 25 %. Good agreement was found for the horizontal position where the fountain impinged upon the interface or the ground, though the radius at the point of impact moderately underpredicted what was observed.

We used two methods to classify the spreading-regimes of flow that result when a fountain in a two-layer fluid returns to the interface through which it initially passed. The theoretical classification compared the density of the return flow at the interface to the density of the lower layer, predicting that the fountain should return to the ground if it was more dense. The agreement between theory and experiment was fairly good considering the simplifying assumptions of the theory. The empirical classification determined whether the fountain was interface-spreading or ground-spreading through two non-dimensional parameters that could be readily computed from source conditions: $\theta = (\rho_2 - \rho_1)/(\rho_2 - \rho_0)$ and H_m/H. We formulated the empirical function $\theta(H_m/H)$ that well separated the regimes. The results were similar to those of fountains in stationary ambients (Ansong *et al.* 2008): if $H_m \lesssim 2H$, the descending flow returned to the level of the source irrespective of θ, but if $H_m \gtrsim 2.5H$, the return flow spread at the interface if $\theta \gtrsim 0.1$.

In both the one- and two-layer experiments, we observed that the initial downstream spreading speeds of currents, whether at the ground or interface, moved at approximately constant speed. However, there was no obvious relationship between this speed and the parameters of the experiment as was found for fountains and plumes in stationary environments (Ansong *et al.* 2008; Ansong & Sutherland 2010). The propagation of gravity currents arising from fountains in both one- and two-layer environments requires further investigation, particularly as these are relevant to the motivating problem of understanding pollutant dispersion in the presence of an atmospheric inversion.

Acknowledgements

We are grateful for the comments of the referees, whose comments helped to improve the manuscript. This work was supported through NSERC's Discovery Accelerator Supplement programme.

REFERENCES

ANSONG, J., KYBA, P. J. & SUTHERLAND, B. R. 2008 Fountains impinging upon a density interface. *J. Fluid Mech.* **595**, 115–139.

ANSONG, J. & SUTHERLAND, B. R. 2010 Internal gravity waves generated by convective plumes. *J. Fluid Mech.* **648**, 405–434.

BODURTHA, J. F. 1961 The behaviour of dense stack gases. *J. Air Pollut. Control Assoc.* **11**, 431–437.

BRIGGS, G. 1969 Plume rise. *Tech. Rep.* TID-25075, NTIS. USAEC Critical Review Series.

BRIGGS, G. A. 1975 Plume rise predictions. In *Lectures on Air Pollution and Environmental Impact Analyses*, pp. 59–111. American Meteorological Society.

BRITTER, R. 1989 Atmospheric dispersion of dense gases. *Annu. Rev. Fluid Mech.* **21**, 317–344.

BRITTER, R. & GRIFFITHS, R. 1982 The role of dense gases in the assessment of industrial hazards. *J. Hazard. Mater.* **6**, 3–12.

CHU, V. 1975 Turbulent dense plumes in a laminar cross flow. *J. Hydraul. Res.* **13**, 263–279.

CHU, V. & GOLDBERG, M. 1974 Buoyant forced-plumes in cross flow. *J. Hydraul. Div. Proc. ASCE* **100**, 1203–1214.

FAY, J. & ZEMBA, S. 1986 Integral model of dense gas plume dispersion. *Atmos. Environ.* **20**, 1347–1354.

GUNGOR, E. & ROBERTS, P. 2009 Experimental studies on vertical dense jets in a flowing current. *J. Hydraul. Engng* **135**, 935–948.

HOOT, T., MERONEY, R. & PETERKA, J. 1973 Wind tunnel tests of negatively buoyant plumes. *Tech. Rep.* US Environmental Protection Agency, Report EPA-650/3-74-003.

HOULT, D., FAY, J. & FORNEY, L. 1969 Theory of plume rise compared with field observations. *J. Air Pollut. Control Assoc.* **19**, 585–590.

HUNT, G. R. & KAYE, N. B. 2005 Lazy plumes. *J. Fluid Mech.* **533**, 329–338.

HUNT, G. R. & KAYE, N. B. 2001 Virtual origin correction for lazy turbulent plumes. *J. Fluid Mech.* **435**, 377–396.

KAYE, N. B. & HUNT, G. R. 2006 Weak fountains. *J. Fluid Mech.* **558**, 319–328.

JOHNSON, M. & KOSTIUK, L. 2000 Efficiencies of low-momentum jet diffusion flames in crosswinds. *Combust. Flame* **123**, 189–200.

KOTSOVINOS, N. 2000 Axisymmetric submerged intrusion in stratified fluid. *J. Hydraul. Engng ASCE* **126**, 446–456.

LANE-SERFF, G., LINDEN, P. & HILLEL, M. 1993 Forced, angled plumes. *J. Hazard. Mater.* **33**, 75–99.

LEE, J. & CHU, V. 2003 *Turbulent Buoyant Jets and Plumes: A Langrangian Approach*. Kluwer Academic.

LINDBERG, W. 1994 Experiments on negatively buoyant jets, with and without cross-flow. In *NATO Advanced Research Workshop on 'Recent Advances in Jets and Plumes'*, NATO ASI Series E, vol. 255, pp. 131–145. Kluwer Academic.

MANINS, P. 1979 Partial penetration of an elevated inversion layer by chimney plumes. *Atmos. Environ.* **13**, 733–741.

MCQUAID, J. 1989 Dispersal of chemicals. In *Methods for Assessing and Reducing Injury from Chemical Accidents* (ed. P. Bourdeau & G. Green), pp. 157–187. Wiley.

MIDDLETON, J. 1986 The rise of forced plumes in a stably stratified crossflow. *Boundary-Layer Meteorology* **36**, 187–199.

MORTON, B. R. 1959 Forced plumes. *J. Fluid Mech.* **5**, 151–163.

MORTON, B. R., TAYLOR, G. I. & TURNER, J. S. 1956 Turbulent gravitational convection from maintained and instantaneous sources. *Proc. R. Soc.* A **234**, 1–23.

ROBERTS, P. & TOMS, G. 1987 Inclined dense jets in flowing currents. *J. Hydraul. Engng* **113** (3), 323–341.

SCHATZMANN, M., SNYDER, W. & LAWSON, R. 1993 Experiments with heavy gas jets in laminar and turbulent cross-flows. *Atmos. Environ.* **27A**, 1105–1116.

SHAVER, E. & FORNEY, L. 1988 Properties of industrial dense gas plumes. *Atmos. Environ.* **22**, 833–837.

SHIAU, B.-S., YANG, C.-L. & TSAI, B.-J. 2007 Experimental observations on the submerged discharge of brine into coastal water in flowing current. *J. Coast. Res.* **50**, 789–793.

TURNER, J. S. 1966 Jets and plumes with negative or reversing buoyancy. *J. Fluid Mech.* **26**, 779–792.

WEIL, J. 1988 Plume rise. In *Lectures on air pollution modelling* (ed. A. Venkatram & J. Wyngaard), pp. 119–166. American Meteorological Society.